

# Supporting Information for: **Pathway-engineering for highly-aligned block copolymer arrays**

*Youngwoo Choo,<sup>1</sup> Paweł W. Majewski,<sup>\*2,3</sup> Masafumi Fukuto,<sup>4</sup> Chinedum Osuji,<sup>\*1</sup> Kevin G.*

*Yager<sup>\*2</sup>*

<sup>1</sup> Department of Chemical Engineering, Yale University, New Haven CT 06511

<sup>2</sup> Center for Functional Nanomaterials, Brookhaven National Laboratory, Upton, NY 11973

<sup>3</sup> Department of Chemistry, University of Warsaw, Warsaw, Poland

<sup>4</sup> National Synchrotron Light Source II, Brookhaven National Laboratory, Upton, NY 11973

\* pmajewski@chem.uw.edu.pl, chinedum.osuji@yale.edu, kyager@bnl.gov

## Ordering of morphology

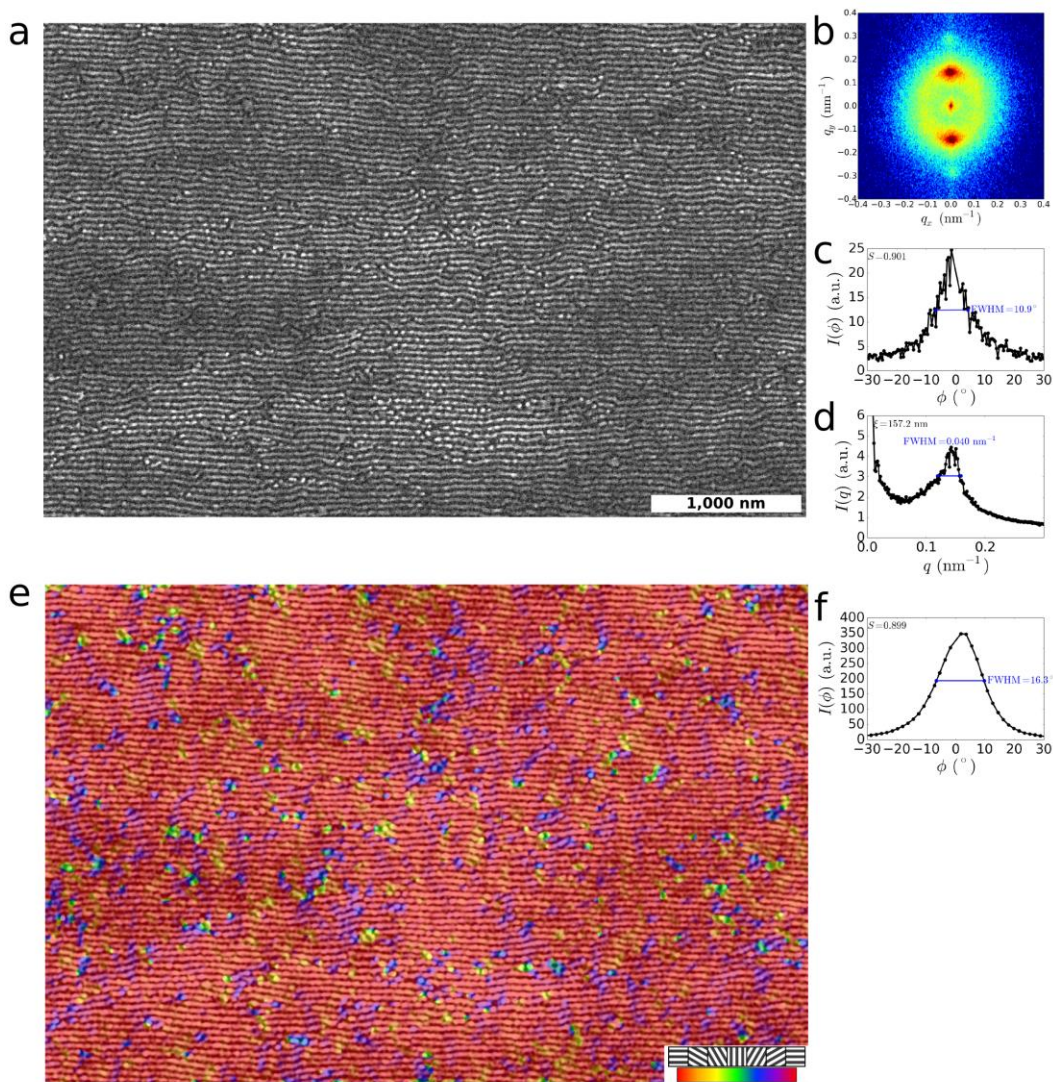


**Figure S1:** Example of highly-aligned horizontal-cylinder state obtained via shearing. Various characterizations via image analysis are shown. The BCP thin film was shear-aligned using a photo-thermal method ( $2\times$  sweeps of SS-LZA at  $80\ \mu\text{m/s}$ ). (a) Scanning Electron Microscopy images demonstrate strong alignment of the morphology, highlighted in the (b) Fourier transform (FFT) of the full image. (c) A linecut through the FFT in the angular ( $\phi$ ) direction can be used to estimate the orientational order from the peak width (FWHM), and the 2D orientational order parameter ( $S$ ).<sup>1</sup> (d) The first-order peak from the one-dimensional circular average of the FFT can be used to estimate a typical correlation length ( $\xi$ ) over which order is preserved. (e) Image gradient analysis can be used to generate a morphology orientation map (false-color representation shown).<sup>2-4</sup> (f) The corresponding histogram of orientations provides an alternate estimate of orientational spread.

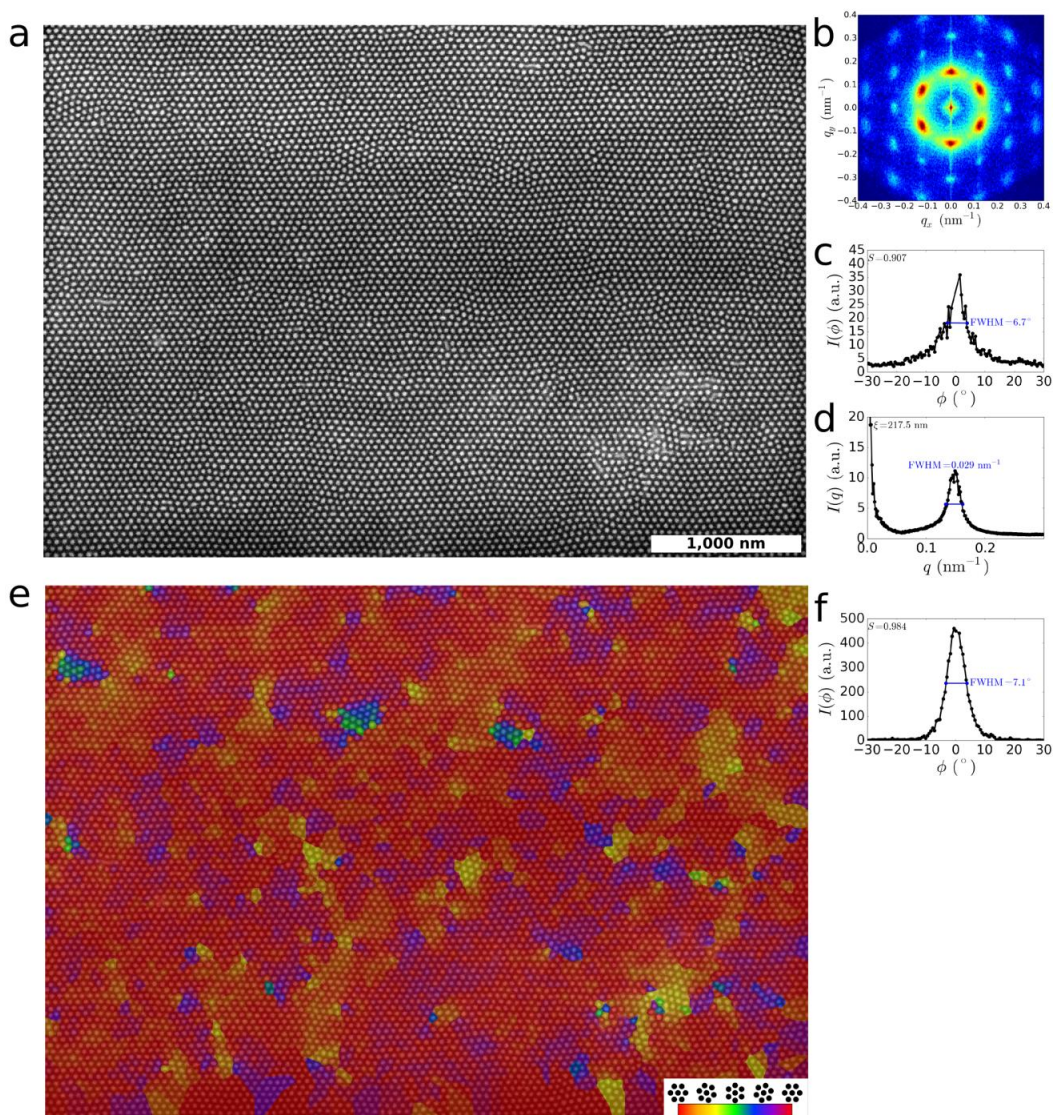


**Figure S2:** Example of highly-aligned vertical-cylinder state obtained via pathway-engineering. The BCP thin film was shear-aligned ( $2\times$  sweeps of SS-LZA at  $80\ \mu\text{m/s}$ ), and subsequently annealed using rapid thermal processing (RTP, 1 min at  $340^\circ\text{C}$ ). The sample was converted to  $\text{AlO}_x$  to improve imaging contrast. (a) Scanning Electron Microscopy images demonstrate excellent alignment of the morphology. (b) Fourier transform (FFT) of the full image demonstrates the preserved alignment (hexagonal peaks) and good long-range order (higher-order peaks). (c) A linecut through the FFT in the angular ( $\phi$ ) direction can be used to estimate the orientational order from the peak width (FWHM), and the 2D orientational order parameter ( $S$ ). (d) The first-order peak from the one-dimensional circular average of the FFT can be used to estimate a typical correlation length ( $\xi$ ) over which order is preserved. (e) Image analysis can be used to identify the cylinder positions, and generate a map of local morphology orientation (false-color representation shown).<sup>5</sup> (f) The corresponding histogram of orientations provides an alternate estimate of orientational spread.

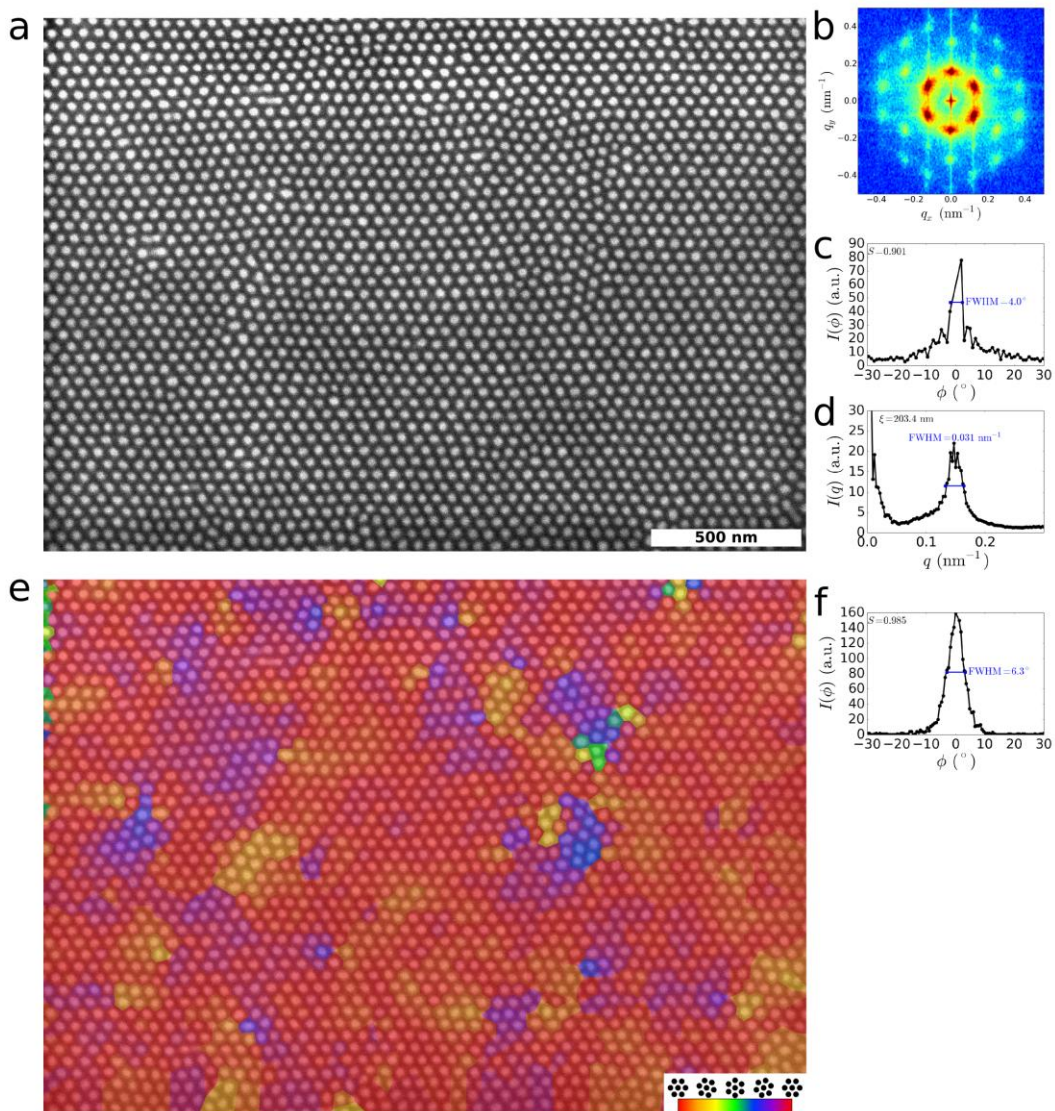


**Figure S3:** Example of highly-aligned vertical-cylinder state obtained via pathway-engineering and optimization of film thickness (32 nm) and annealing temperature. The BCP thin film was shear-aligned ( $2\times$  sweeps of SS-LZA at  $80 \mu\text{m/s}$ ), and subsequently annealed using rapid thermal processing (RTP, 1 min at  $320^\circ\text{C}$ ). The sample was converted to  $\text{AlO}_x$  to improve imaging contrast.

## Reorientation

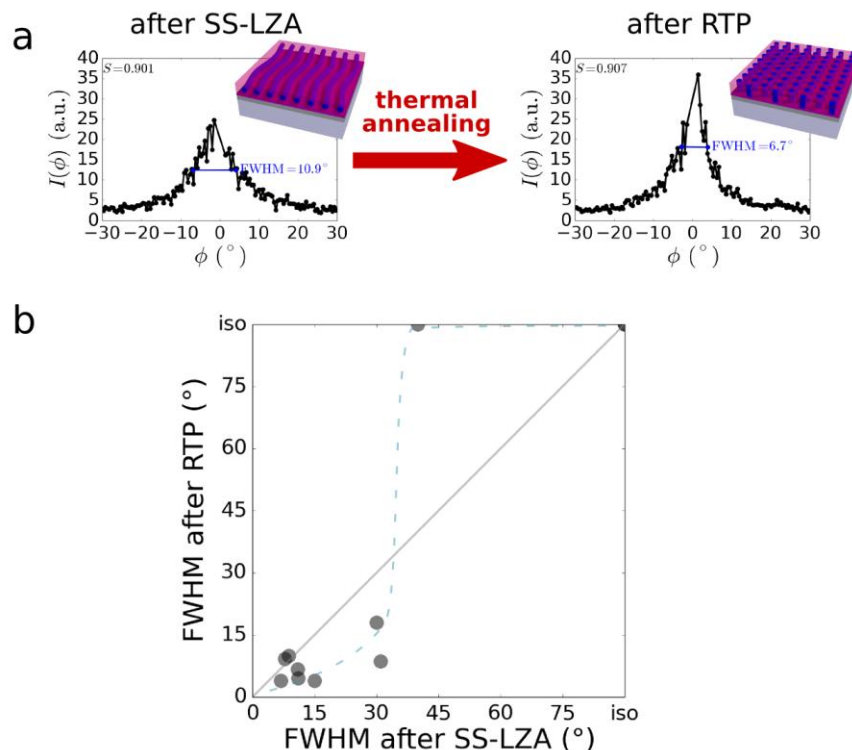


**Figure S4:** (a) Example of the change in orientational spread upon thermal annealing, which converts the morphology from horizontal to vertical cylinders. (b) Correlation between orientational spread of morphology after SS-LZA (i.e. the orientation of the horizontal cylinders with respect to the shear direction) and the orientational spread after RTP (i.e. the orientation of the hexagonal domains). A collection of results across different experimental conditions (described in main text) are plotted; isotropic (iso) ordering is defined as orientational  $\text{FWHM} = 90^\circ$ . The grey line represents the case where the templated state exactly reproduces the orientational spread of the original state. Surprisingly, across a broad range of conditions, the order is found to be *greater* (i.e. smaller orientational  $\text{FWHM}$ ) after RTP conversion from the horizontal to vertical state. While the templated state clearly inherits the order of the shear-aligned state, the reordering evidently improves order and anneals away defects (e.g. undulations) in the original state. The available data also suggest that the shear-aligned state must exhibit sufficient anisotropy ( $\text{FWHM} < 40^\circ$ ) for the templating to be effective (dashed line is a guide to the eye).

film thickness (nm)	Shear (SS-LZA) Processing					RTP Processing					
	velocity (mm/s)	sweeps	FWHM (°)	S	defect density ( $\mu\text{m}^{-2}$ )	T (°C)	$f_{\text{perp}}$	FWHM (°)	S	$f_{6\text{NN}}$	defect density ( $\mu\text{m}^{-2}$ )
30	0.32	4x	iso	0.000	385.6	320	1.00	iso	0.000	0.63	74.1
30	0.32	16x	31.0	0.787	183.7	320	1.00	8.6	0.974	0.88	23.9
30	0.32	64x	30.0	0.912	160.0	320	1.00	18.4	0.906	0.75	49.4
30	5.12	2x	iso	0.000	347.9	320	0.91	iso	0.000	0.07	186.1
30	2.56	2x	39.8	0.573	311.4	320	0.98	iso	0.000	0.11	152.0
30	1.28	2x	8.8	0.915	167.8	320	1.00	10.0	0.974	0.87	25.8
30	0.08	2x	10.9	0.899	202.7	340	1.00	6.7	0.984	0.94	12.7
30	0.08	2x	7.8	0.862	297.7	320	1.00	9.2	0.981	0.93	15.4
32	0.08	2x	6.8	0.920	108.3	320	1.00	<b>4.0</b>	<b>0.987</b>	<b>0.97</b>	<b>7.1</b>
36	0.08	2x	11.3	0.961	32.3	320	1.00	4.6	0.983	0.93	14.7
40	0.08	2x	15.2	0.870	91.9	320	1.00	4.0	0.977	0.78	47.3

**Table S1:** Different measures of order for different processing histories, including both the initial shear-alignment (SS-LZA) and final thermal annealing (RTP) steps. SS-LZA is defined by translation velocity and number of sweeps. The ordered state after this step (nominally a monolayer of horizontal cylinders aligned along the shear direction) can be characterized by the orientational spread of the morphology with respect to the shear direction (FWHM, based on FFT), the orientational order parameter ( $S$ , based on morphology orientation map), or the defect density (calculated via particle counting image analysis, since breaks in the morphology lines represent defects). RTP is defined by the processing temperature ( $T$ ). The ordered state after this step (nominally a hexagonal array of cylinders) can be characterized by the fraction of perpendicular (vertical) cylinders ( $f_{\text{perp}}$ ), the orientational spread of the morphology (FWHM), the orientational order parameter ( $S$ ), the fraction of cylinders exhibiting six nearest-neighbors ( $f_{6\text{NN}}$ ),<sup>5</sup> or the defect density (calculated by summing contributions from horizontal-cylinder regions and cylinders that do not have precisely six nearest-neighbors). The various metrics probe different aspects of ordering; nevertheless, there is considerable correlation between these measures (best-ordered final state in bold).

T (°C)	$f_{\text{perp}}$	FWHM (°)	S	$f_{6\text{NN}}$	defect density ( $\mu\text{m}^{-2}$ )
190	0.68	19.4	0.873	0.02	158.5
220	0.66	14.4	0.926	0.14	294.3
250	0.91	iso	0.000	0.17	192.0
300	1.00	iso	0.000	0.32	134.5

**Table S2:** Measures of order for different RTP processing conditions. For the presented data, the initial SS-LZA processing was performed using  $T_b = 120^\circ\text{C}$ , and processing using 2x sweeps at  $320 \mu\text{m/s}$ . Control of the RTP thermal annealing step strongly influences the reorientation to vertical cylinders ( $f_{\text{perp}}$ ), while also affecting other aspects of order.

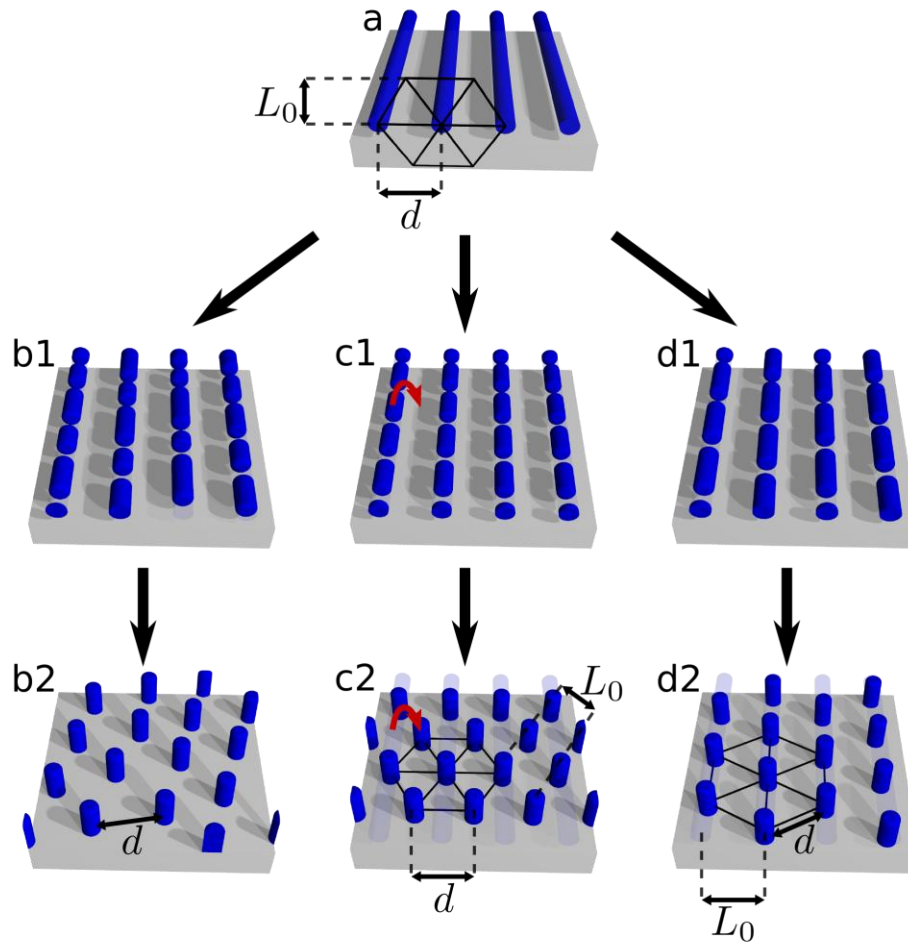


**Figure S5:** Templated reorientation of a BCP cylinder phase. A monolayer of horizontal cylinders (a) has the cylinders spaced in-plane according to the cylinder-cylinder distance ( $d$ ). A multi-layer would add additional rows of cylinders layered by  $L_0 = d \times \sqrt{3} / 2$  in the film normal direction. This horizontal state could potentially reorient into a vertical cylinder state in a variety of ways (b, c, d). If the breakup of cylinder is essentially random (b1), the corresponding vertical cylinder state (b2) will not be templated by the initial state. It will exhibit the usual preferred morphological lengthscale ( $d$ ), but no templated registry. Arguably, the most natural orientation of the final vertical cylinder state is that which aligns the cylinder-cylinder distance ( $d$ ) in the same direction as the initial cylinder-cylinder repeat (c2). However, this reorientation process (c1) involves the motion of a substantial amount of BCP material (e.g. region denoted by red arrow). What is observed experimentally is instead that horizontal cylinders breakup in a coordinated and ‘out-of-phase’ manner in adjacent cylinder rows (d1), such that the final vertical cylinder rows align along the initial horizontal cylinder long-axes (d2). This involves a minimal amount of reorganization of the underlying block copolymer chains. Notably, this requires a reasonable match between the horizontal cylinder spacing ( $d$ ) and the vertical cylinder row spacing ( $L_0$ ); though a modest mismatch can be accommodated through distortion of the polymer chain conformations.

## Energy landscape

The characteristic shape of the energy landscape for BCP ordering can be estimated by considering the dominant driving forces for ordering. For the present set of reordering experiments, the principal energetic drivers are: (1) phase separation of the two BCP components, (2) the in-plane (IP) vs. out-of-plane (OOP) orientation of the system, (3) the in-plane order. Phase separation is characterized by the Flory-Huggins interaction parameter,  $\chi$ , which has a temperature-dependence owing to a balance between entropic ( $\chi_s$ ) and enthalpic ( $\chi_H$ ) contributions:

$$\chi(T) = \chi_s + \frac{\chi_H}{T} \quad (1)$$

The material studied herein (PS-*b*-PMMA) has a relatively weak temperature-dependence:<sup>6</sup>  $\chi_s = 0.028$ ,  $\chi_H = 3.9$ . The interfacial width in BCP phases,  $W$ , is dictated by this segregation strength<sup>7-9</sup> via  $W = 1/\sqrt{6\chi}$ , where  $a$  is the polymer statistical segment length. We can thus write:

$$T = \frac{\chi_H}{\left(a^2 / 6W^2 - \chi_s\right)} \quad (2)$$

This describes the temperature require to thermally-broaden the BCP interfaces to a breadth  $W$ . As done previously, we postulate an energetic term of a similar form (multiplied by  $k_B$ ), to describe the energy penalty inherent to states where phase-separation has not occurred (in particular, the initially disordered state obtained after spin-casting):<sup>10,11</sup>

$$E_W = \frac{k_B \chi_H}{\left(a^2 / 6W^2 - \chi_s\right)} \quad (3)$$

With respect to in-plane order, we quantify order using the correlation length ( $\xi$ ), which can be thought of as a characteristic grain size (distance over which the morphological orientation is preserved). The correlation length is inversely related to defect density,  $\rho_d = N_d / A \sim 2 / (L_0 \xi)$ , where  $N_d$  is the number of defects and  $A$  is the film area. The energetic contribution along this axis is a succession of energy barriers, with total energy decreasing with each defect annihilation event ( $E_\xi = N_d E_d$ ). Each defect incurs an energy penalty ( $E_d$ ) of order 10–150  $k_B T$ , while elimination of a defect involves overcoming 1–4 barriers of height  $\sim 1$ –20  $k_B T$ .<sup>10,12,13</sup> With respect to OOP orientation, we assume a single energy barrier, with the vertical orientation being ultimately lower energy. For simplicity, we model the energetics of orientation using an ad-hoc energy term of the form:

$$E_{\text{OOP}} = c_1 k_B f_{\text{perp}}^2 + c_2 k_B \exp \left[ - \frac{\left(f_{\text{perp}} - 1/2\right)^2}{\sigma_{\text{OOP}}} \right] \quad (5)$$

Where the  $c$ , and  $\sigma_{\text{OOP}}$ , are constants. We note that it is likely that the energy terms for defect annihilation and reorientation depend on  $W$ ; in particular, when materials are weakly segregated (large  $W$ ), the energy barriers for reorganization are expected to be smaller. We model the overall state energy using the sum of the above effects ( $E_W + E_\xi + E_{\text{OOP}}$ ). The presented diagrams are computed using the above equations and assumptions; however scaling is selected in an ad hoc manner in order to highlight the expected structure of the energy landscape. While these diagrams should be taken as schematic only, they help to visualize the multi-dimensional energy space.

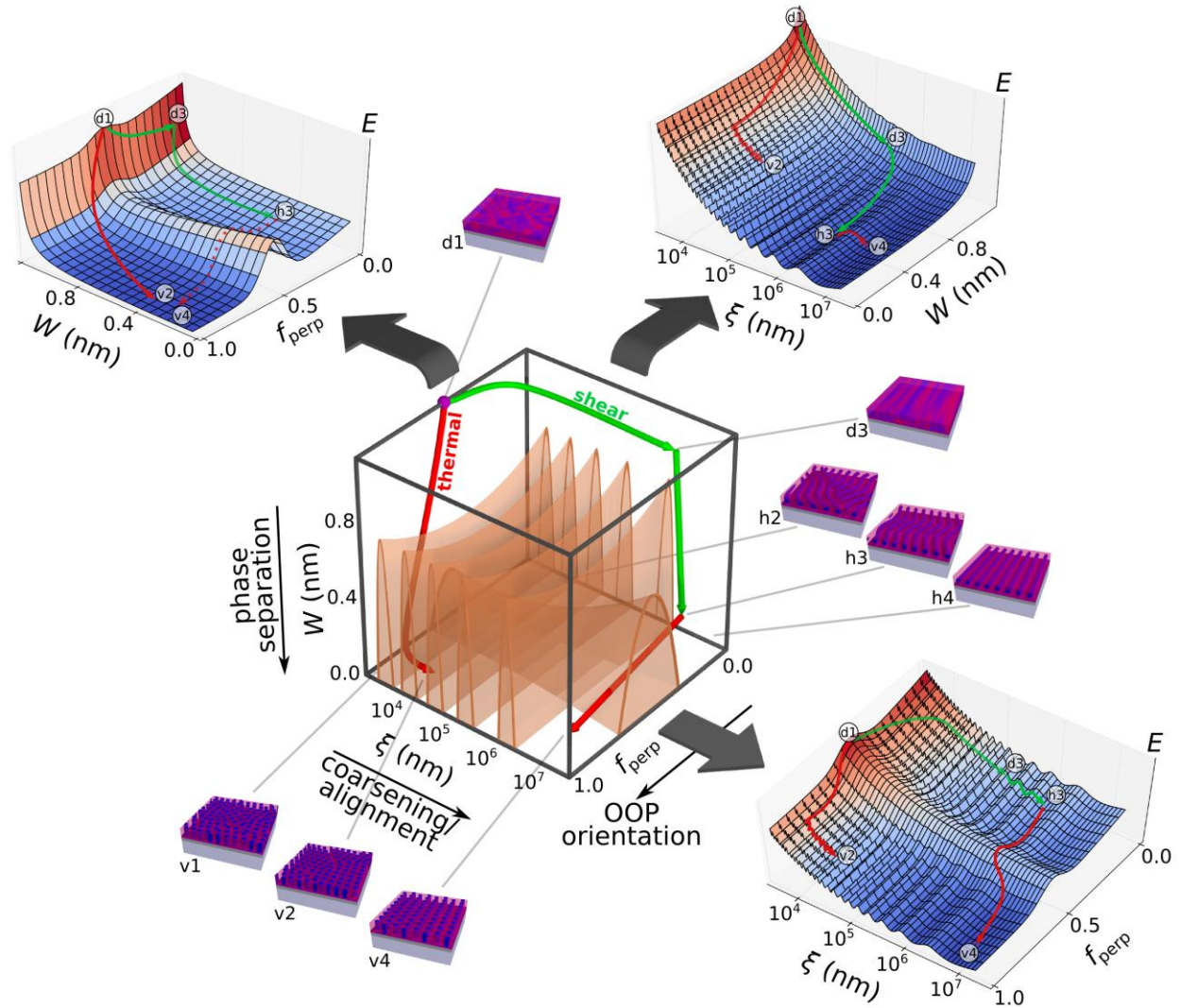


**Figure S6:** Schematic of pathway-dependent ordering in a multi-dimensional energy landscape. The energy surfaces ( $E$ ) are based on the expected energy contributions, but are scaled in an ad-hoc manner to highlight the structure of the landscape. The overall parameter space (central cube) is represented based on three dominant effects: (1) The strong driving force towards phase separation of the two BCP components is characterized by the interfacial width ( $W$ ); (2) the out-of-plane (OOP) orientation of the system is quantified by the fraction of perpendicular domains ( $f_{\text{perp}}$ ), where (for the substrate conditions studied here) the system will preferentially form perpendicular (vertical cylinder) domains, with an energy barrier for reorientation; (3) the in-plane order is characterized by the grain size ( $\xi$ ), where in the limit of large grains one is instead considering the orientational spread (alignment) of the system. The energy landscape is characterized by a set of energy barriers (shown as orange volumes), which limit reordering. Efficient pathways through this ordering space can be selected in order to generate a targeted final structure. An as-cast film is disordered ( $d1$ ). Thermal annealing (red arrow) begins with rapid phase separation, which kinetically traps the system in a poorly-ordered state mired by energy barriers ( $v1$ ,  $v2$ ). Conversely, an ordering pathway that begins with shearing (green arrow) first breaks symmetry ( $d3$ ), then generates an ordered horizontal state ( $h3$ ), which is ideally-situated to be thermally converted into a highly-ordered vertical state ( $v4$ ).

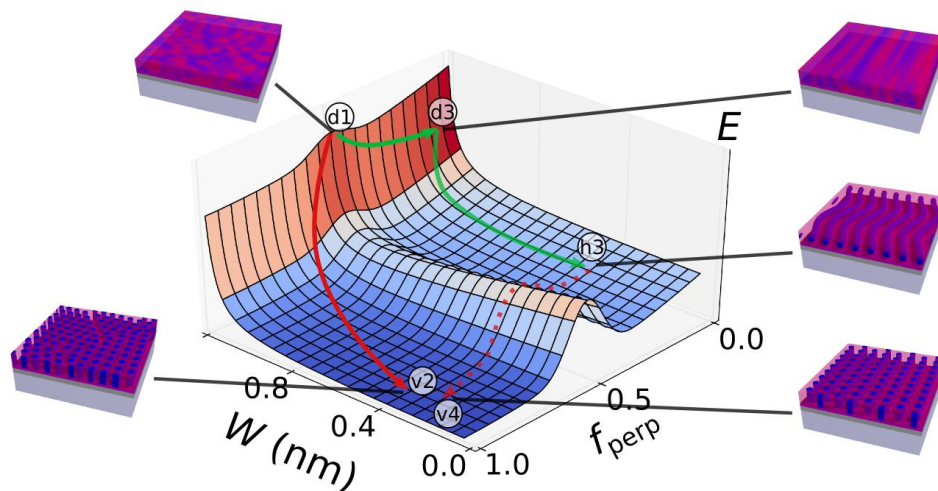


**Figure S7:** Schematic of the energy landscape for ordering of a BCP thin film of cylinder morphology, with respect to phase separation and orientation. Phase separation is characterized by the interfacial width between domains ( $W$ ), while the orientation is characterized by  $f_{\text{perp}}$ ;  $f_{\text{perp}} = 0$  indicates a parallel orientation (horizontal cylinders), while  $f_{\text{perp}} = 1$  indicates a perpendicular orientation (vertical cylinders). The as-cast film is disordered and thus high-energy (d1). Thermal annealing (red arrow) involves rapid demixing of the two components ( $W$  decreasing rapidly). The system naturally proceeds towards the vertical cylinder morphology. The extreme driving force of shearing (green) breaks symmetry and drives the system towards  $f_{\text{perp}} = 0$  (d3). Continued photo-thermal shearing allows the system to phase-separated ( $W$  decreasing), while always enforcing a horizontal alignment of the morphology (h3). Subsequent thermal annealing from this state generates a vertical cylinder morphology templated from the aligned horizontal morphology; thus this templated state is highly ordered (v4). The thermal pathway from the horizontal to vertical state involves crossing an energy barrier for reorientation (pathway shown with dashed red arrow to emphasize that this pathway—and the final state v4—are in a different portion of the 3D landscape).

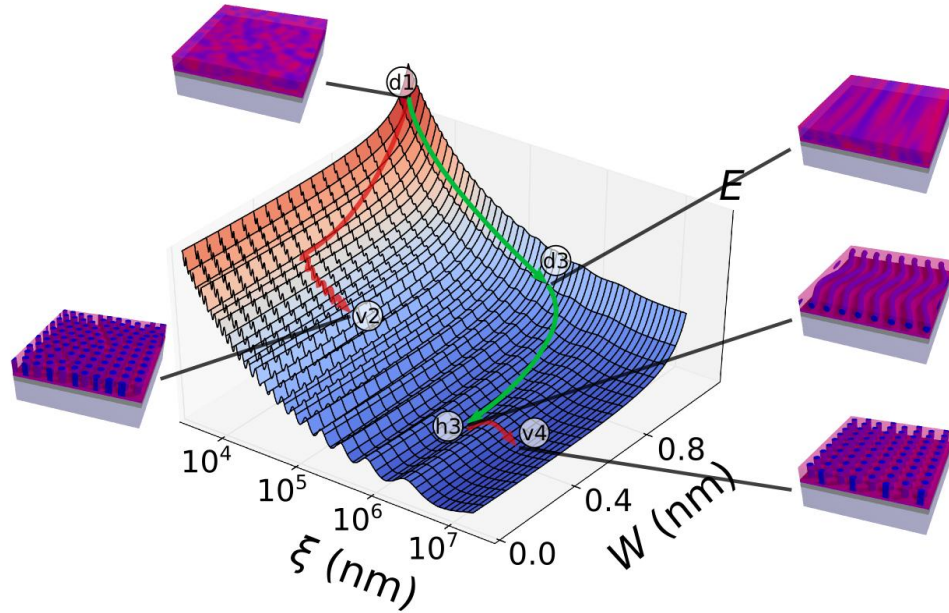


**Figure S8:** Schematic of the energy landscape, with respect to phase separation ( $W$ ) and coarsening (denoted by grain size,  $\xi$ ). For the present purposes, grain size and overall alignment are treated as related. That is, the limit of large grains represents a highly-aligned state (same orientation throughout sample); conversely angular spread in an aligned phase can be characterized as a decrease in the correlation length. Starting from a disordered as-cast state (d1), thermal annealing (red arrow) induces rapid phase separation. This generates well-defined local morphology, but with multiple grains at different orientations. Grain coarsening requires diffusion and annihilation of topological defects, a process that involves a succession of energy barriers. The system is thus kinetically trapped in the poly-grain portion of the landscape (v2). Conversely, rapid shearing (green arrow) aligns the system before phase separation can complete (d3). Continued photo-thermal shearing allows the system to phase separate and relax into a well-aligned morphology (h3). Subsequent thermal annealing allows the system to reorient (horizontal to vertical) in a way that retains the in-plane alignment. This templated reorientation thus gives rise to a highly-aligned vertical cylinder state (v4).

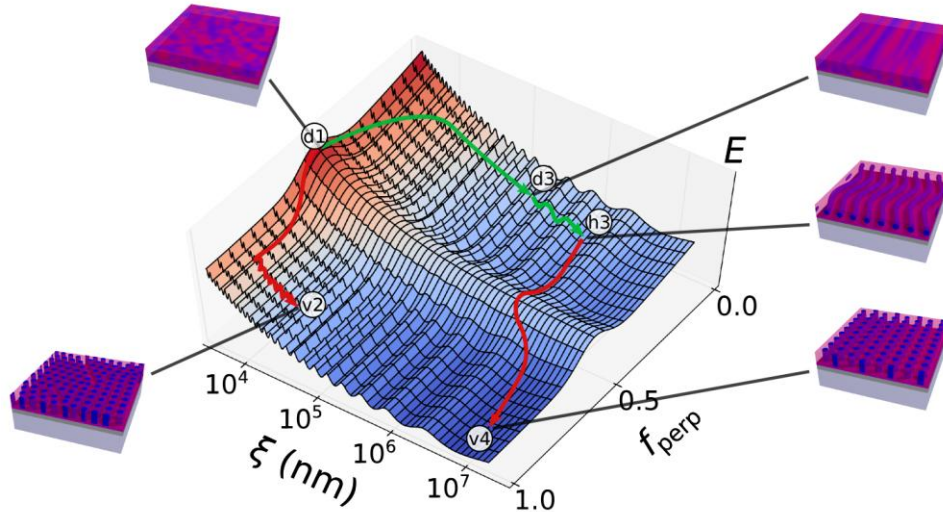


**Figure S9:** Schematic of the energy landscape, with respect to grain size ( $\xi$ ), and out-of-plane orientation ( $f_{\text{perp}}$ ). Thermal annealing (red arrow) of an as-cast state (d1) causes the system to form a vertical-cylinder state (since this configuration is lower-energy overall, given the neutral substrate conditions considered here). However, such a state is kinetically trapped by a succession of energy barriers for defect annihilation. Thus even with substantial thermal annealing, the morphology is a vertical orientation of cylinder domains with small grain size (poly-grain, v2). Shearing (green arrow) instead forces the system towards the horizontal-cylinder part of the phase diagram (in the 3D landscape, one can see how this bypasses energy barriers). Continued shearing orders the system into well-define horizontal cylinders aligned along the shear direction (h3). Subsequent thermal processing allows the system to overcome the energy barrier for reorientation, forming an aligned vertical cylinder state (v4). This vertical state (v4) is templated from the parent horizontal state (h3). Interestingly, the final state (v4) can be better ordered (smaller orientational spread of morphology) than the parent state (h3). This can be understood in the sense that during reorientation (crossing an energy barrier), the system has the opportunity to heal defects and find lower-energy configurations.

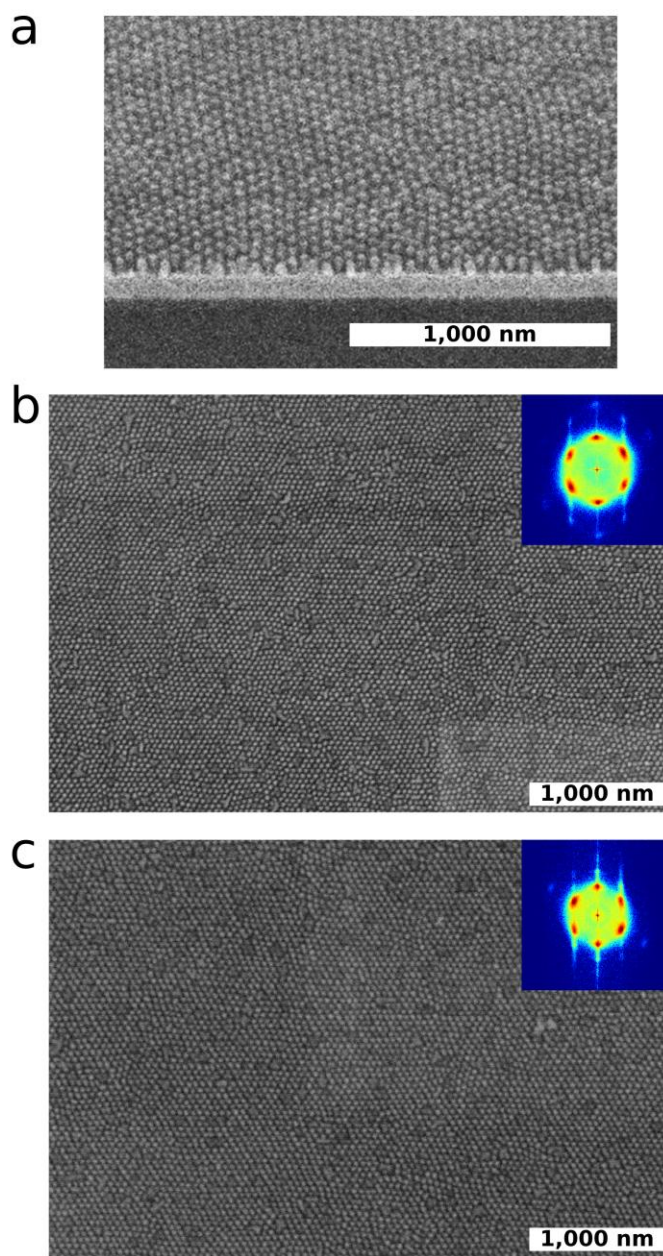


**Figure S10:** Examples of Ge nanopatterns obtained by using an engineered BCP phase as an mask to etch a Ge layer. (a) Tilt-view SEM, where the three-dimensional shape of the resulting Ge nano-pillars can be seen. (b, c) Top-view SEMs of Ge nanopatterns (with corresponding FFT of wide-area image) demonstrate that the Ge nanopattern faithfully inherits the alignment and order of the original organic phase.

## Supporting references

1. P. W. Majewski and K. G. Yager, *J. Phys.: Condens. Matter*, 2016, **28**, 403002.
2. B. C. Berry, A. W. Bosse, J. F. Douglas, R. L. Jones and A. Karim, *Nano Lett.*, 2007, **7**, 2789-2794.
3. K. G. Yager, N. J. Fredin, X. Zhang, B. C. Berry, A. Karim and R. L. Jones, *Soft Matter*, 2010, **6**, 92-99.
4. P. W. Majewski and K. G. Yager, *ACS Nano*, 2015, **9**, 3896-3906.
5. P. W. Majewski and K. G. Yager, *Soft Matter*, 2016, **12**, 281-294.
6. T. P. Russell, R. P. Hjelm and P. A. Seeger, *Macromol.*, 1990, **23**, 890-893.
7. F. Schmitz, P. Virnau and K. Binder, *Phys. Rev. E*, 2014, **90**, 012128.
8. D. F. Sunday and R. J. Kline, *Macromol.*, 2015, **48**, 679-686.
9. U. K. Chaturvedi, U. Steiner, O. Zak, G. Krausch and J. Klein, *Phys. Rev. Lett.*, 1989, **63**, 616-619.
10. P. W. Majewski and K. G. Yager, *Nano Lett.*, 2015, **15**, 5221-5228.
11. S. Samant, J. Strzalka, K. G. Yager, K. Kisslinger, D. Grolman, M. Basutkar, N. Salunke, G. Singh, B. Berry and A. Karim, *Macromol.*, 2016, **49**, 8633-8642.
12. B. Kim, N. Laachi, K. T. Delaney, M. Carilli, E. J. Kramer and G. H. Fredrickson, *J. Appl. Polym. Sci.*, 2014, **131**, 40790.
13. H. Takahashi, N. Laachi, K. T. Delaney, S.-M. Hur, C. J. Weinheimer, D. Shykind and G. H. Fredrickson, *Macromol.*, 2012, **45**, 6253-6265.